Editors' Suggestion | Featured in Physics

Catastrophic Phase Inversion in High-Reynolds-Number Turbulent Taylor-Couette Flow

Dennis Bakhuis,[1] Rodrigo Ezeta,[1] Pim A. Bullee,[1,2] Alvaro Marin,[1] Detlef Lohse,[1,3,*] Chao Sun,[4,5,†] and Sander G. Huisman[1,‡]

[1]*Physics of Fluids Group, Max Planck UT Center for Complex Fluid Dynamics, MESA+ Institute and J.M. Burgers Centre for Fluid Dynamics, University of Twente, 7500 AE Enschede, Netherlands*

[2]*Soft matter, Fluidics and Interfaces, MESA+ Institute for Nanotechnology, University of Twente, 7500 AE Enschede, Netherlands*

[3]*Max Planck Institute for Dynamics and Self-Organization, Am Faßberg 17, 37077 Göttingen, Germany*

[4]*Center for Combustion Energy, Key Laboratory for Thermal Science and Power Engineering of Ministry of Education, Department of Energy and Power Engineering, Tsinghua University, Beijing 100084, China*

[5]*Department of Engineering Mechanics, School of Aerospace Engineering, Tsinghua University, Beijing 100084, China*

(Received 1 October 2020; accepted 17 December 2020; published 11 February 2021)

Emulsions are omnipresent in the food industry, health care, and chemical synthesis. In this Letter the dynamics of metastable oil-water emulsions in highly turbulent ($10^{11} \leq \mathrm{Ta} \leq 3 \times 10^{13}$) Taylor-Couette flow, far from equilibrium, is investigated. By varying the oil-in-water void fraction, catastrophic phase inversion between oil-in-water and water-in-oil emulsions can be triggered, changing the morphology, including droplet sizes, and rheological properties of the mixture, dramatically. The manifestation of these different states is exemplified by combining global torque measurements and local *in situ* laser induced fluorescence microscopy imaging. Despite the turbulent state of the flow and the dynamic equilibrium of the oil-water mixture, the global torque response of the system is found to be as if the fluid were Newtonian, and the effective viscosity of the mixture was found to be several times bigger or smaller than either of its constituents.

DOI: 10.1103/PhysRevLett.126.064501

Mixtures of oil and water are omnipresent in petrochemical processes [1], pharmaceutics [2], as well as in the food industry [3]. For example, in oil recovery, water is generally used as a carrier liquid to extract oil from the ground, creating an emulsion [4]. Also in the further processing of the crude oil, and the synthesis of other chemical compounds, emulsions are a common occurrence. As water and oil are immiscible, due to their polar and nonpolar nature, respectively, they fully separate in two phases. However, when vigorously stirred by turbulence, they can be dispersed into each other. One phase is fragmented to form drops (becoming the dispersed phase) and suspended inside the other liquid (continuous phase), creating an emulsion. Simple emulsions come in two forms: oil droplets suspended in water *(o-w)* or water droplets suspended in oil *(w-o)*. Without continuous stirring, however, both types of emulsions are unstable as density differences and buoyancy promote coalescence of the dispersed phase, causing the two phases to separate. Depending on the application, emulsifiers (stabilizers, surfactants, polymers, or an amphiphile) can be added to gain stability against coalescence—frequently done in the food industry using, e.g., egg yolk or its active component lecithin. Mayonnaise may be the most famous example of such a stabilized emulsion.

In various industrial processes, emulsions are pumped through pipes [5] and stirred in tanks, and determining the rheological properties of these emulsions in these turbulent flow conditions is hard. Conventional rheometers work in the laminar regime such that their flow profile can be easily derived and used for calibration. However, emulsions, without stabilizers, would quickly phase separate in such rheometers, therefore not accurately replicating the metastable state—a state far from equilibrium—that the emulsion has in a turbulent flow. In such turbulent flow of a metastable emulsion, the dispersed phase is continuously broken up by the eddies while at the same time drops continuously coalesce, creating a dynamic equilibrium. Stopping the energy input quickly destroys the dynamic equilibrium and the phases separate.

The theory of the breakup of droplets in a turbulent flow was pioneered by Kolmogorov [6] and Hinze [7]. Their focus was to determine a correlation between the flow scales and the average droplet diameter by dimensional analysis. Turbulent eddies with a scale similar to the droplet can destabilize the interfaces, leading to the breakup of droplets [8]. While the smallest scale in a turbulent flow, i.e., the Kolmogorov scale η_K, was hypothesized as the lower bound for the droplet diameter, it was experimentally found that a portion of droplets can have a smaller size [9]. At these scales (viscous subrange), subeddy viscous stresses dominate over inertial stresses, making smaller droplets possible [10,11].

The stability of an emulsion is not only dictated by the presence of a suitable emulsifier, but also the relative

volume fractions are important. For increasing oil fractions, it becomes harder and harder to maintain an oil-in-water emulsion (without using an emulsifier), and finally oil and water switch their roles and the system undergoes a so-called phase inversion [12,13] to the water droplet in oil case. Various attempts at modeling the inversion point of this phase inversion have been undertaken: minimal dissipation models [14,15], energy barrier models [16], or coalescence and breakup models [17,18]. The critical inversion point of *o-w* to *w-o* and *w-o* to *o-w* is generally not at the same oil volume fraction, i.e., hysteresis is observed [17–20]. According to an extended Ginzburg-Landau model [16], the width of the hysteresis region, also known as the ambivalence region, is a unique property of the emulsion mixture and independent of the Reynolds, Froude, and Weber numbers of the system. Lastly, the typical timescale of the inversion can vary between several days, or being nearly instantaneous; in the latter case the phase inversion is called a *catastrophic* phase inversion [21–23].

In this Letter we investigate the dynamic phase stability and the rheological properties of an unstable emulsion without emulsifiers in highly turbulent shear flow. To do so, we make use of recent advances [24,25] in large scale turbulent Taylor-Couette (TC) facilities, which make it possible to use this geometry as a rheometer—classically solely used in the laminar regime—even in the turbulent regime.

We employ the Twente Turbulent Taylor-Couette facility [24], as it provides local and global measurement access in a controlled and closed geometry, see Fig. 1(a). The apparatus has an inner cylinder (IC) radius $r_{\mathrm{IC}} = 200$ mm, an outer cylinder (OC) radius $r_{\mathrm{OC}} = 279.4$ mm, and a height L=927mm, resulting in a gap width $\delta = 79.4$ mm, a radius ratio $\eta = r_{\mathrm{IC}}/r_{\mathrm{OC}} = 0.716$, and an aspect ratio $\Gamma = L/\delta = 11.7$. The torque, $\mathcal{T}$, required to rotate the IC at constant angular velocity ω_{IC} is measured using a torque sensor. The temperature of the fluids is kept within $21.0 \pm 0.5\,^{\circ}\mathrm{C}$. Optical access to the flow is through a window on top of the system, modified to hold a 200 μm thick microscope slide, thereby allowing us to operate a microscopy system [shown in Fig. 1(b)]. The microscopy system consists of laser induced fluorescence (LIF) lighting, a half-mirror, 20× magnification lens, and a camera [26]. We make use of demineralized water and a low-viscosity silicone oil [27] with $\nu_o = 1.03\ \mathrm{mm^2\,s^{-1}}$ at 25 °C and an interfacial tension with water of $\gamma = 42.7\ \mathrm{mNm^{-1}}$ [28].

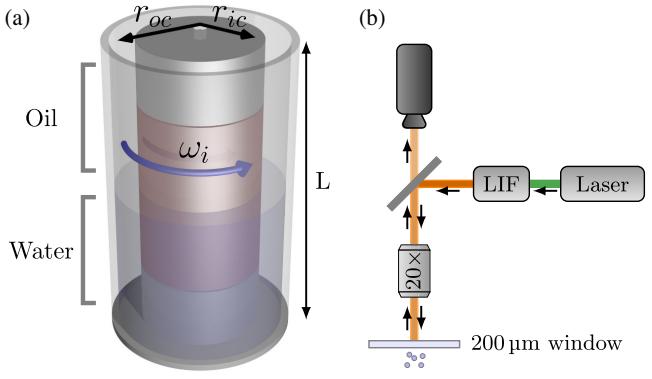

FIG. 1. (a) Schematic of the T^{3}C setup. Initially, the water (bottom) and oil (top) are separated. (b) *In situ* high-speed microscopy using LIF lighting, a half-mirror, and a 20× magnification lens, through a 200 μm thick window at the top of the setup shown in (a).

The driving strength of TC flow can be quantified by the Taylor number [29]:

$$\mathrm{Ta} = \frac{1}{4}\sigma\delta^2(r_{\mathrm{IC}} + r_{\mathrm{OC}})^2(\omega_{\mathrm{IC}} - \omega_{\mathrm{OC}})^2/\nu^2 \qquad (1)$$

where $\sigma = [(1+\eta)/(2\sqrt{\eta})]^4$ is a geometric constant. The response of the system, the torque, can then be captured as an angular velocity Nusselt number [29]:

$$\mathrm{Nu}_\omega \equiv \frac{J_\omega}{J_\omega^{\mathrm{lam}}} = \frac{\mathcal{T}}{2\pi L\rho J_\omega^{\mathrm{lam}}}. \qquad (2)$$

Here $J_\omega^{\mathrm{lam}} = 2\nu r_{\mathrm{IC}}^2 r_{\mathrm{OC}}^2(\omega_{\mathrm{IC}} - \omega_{\mathrm{OC}})/(r_{\mathrm{OC}}^2 - r_{\mathrm{IC}}^2)$ is the angular velocity transport for laminar, nonvortical flow. From dimensional analysis $\mathrm{Nu}_\omega = f(\mathrm{Ta}, \omega_{\mathrm{OC}}/\omega_{\mathrm{IC}}, \Gamma, \eta)$, where f is some general function, which has been experimentally found and numerically verified [25,30–34]. We keep η and Γ constant and the OC remains stationary, $\omega_{\mathrm{OC}} = 0$, such that we have $\mathrm{Nu}_\omega = f(\mathrm{Ta})$.

In order to compute an effective viscosity for a metastable emulstion (MSE), we will assume that the system globally responds as if it were filled with a Newtonian liquid at these shear rates. While quasistatically ramping up the inner cylinder from $\omega_{\mathrm{IC}}/(2\pi) = 4$ Hz to 20 Hz, the torque $\mathcal{T}$ was measured for various oil volume fractions $\alpha = V_o/(V_o + V_w)$, where V_o (V_w) is the volume of the oil (water) phase. Experiments based on liquids with known viscosity define the curve $\mathrm{Nu}_\omega = f(\mathrm{Ta})$ for our geometry, which we do so using the $\alpha = 0\%$ and $\alpha = 100\%$ cases. The scaling of $\mathrm{Nu}_\omega = f(\mathrm{Ta})$ can now be exploited to determine $\nu_{\mathrm{eff}}(\alpha)$ such as to collapse all the data on to a single curve. Indeed, all 32 datasets collapse onto a single universal curve (see Fig. 2), consistent with previous studies on Newtonian liquids and emulsions [30,31,33–39]. To appreciate the quality of the collapse, all data were compensated by $\mathrm{Ta}^{0.4}$, which is the effective scaling around $\mathrm{Ta} = \mathcal{O}(10^{12})$ (inset of Fig. 2). This analysis shows that all datasets combined have a standard deviation of only 1.2%, and that the expected scaling is also around $\mathrm{Nu}_\omega \propto \mathrm{Ta}^{0.4}$, which justifies the Newtonian assumption made earlier for the MSE at such large shear rates.

The effective viscosity $\nu_{\mathrm{eff}}(\alpha)$, normalized using the viscosity of water ν_w, is shown in Fig. 3 as blue circles. Each experimental measurement in this set is performed at

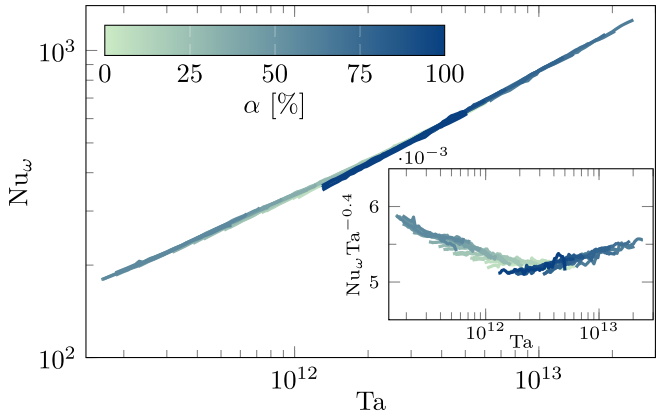

FIG. 2. Nu_ω as a function of Ta for a total of 32 experiments. By exploiting the relation between $\mathrm{Nu}_\omega = f(\mathrm{Ta})$, an effective viscosity ν_{eff} was found for each experiment such that all the datasets collapse on a single curve, by minimizing $\sigma(\mathrm{Nu}_\omega)$ for the collective data, binned in Ta. The inset shows the compensated datasets, revealing the overlap within a couple of percent. The colors of the lines indicate the oil fraction.

a constant oil fraction α, while ensuring that the two phases were fully mixed, and is depicted as "fixed α" in the figure. We observe two disconnected branches, the left branch for $\alpha \leq 65\%$, and the right branch for $\alpha \geq 70\%$, corresponding to *o-w* and *w-o* emulsions, respectively. Remarkably, we find that by adding oil (á) the effective viscosity increases *beyond* the viscosities of each of the constituents, making the fluid three times as viscous as water for $\alpha = 65\%$.

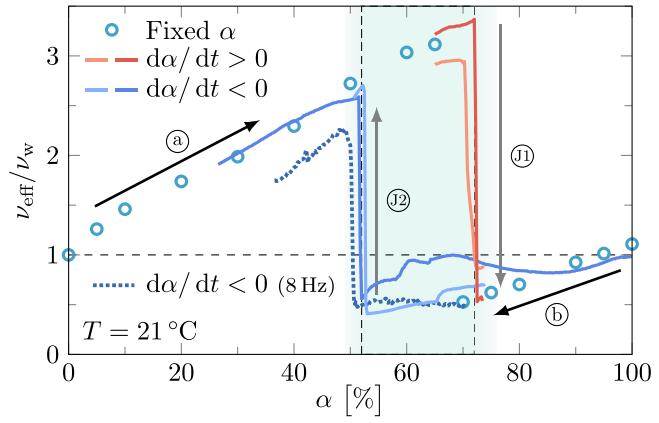

FIG. 3. Effective viscosity normalized by the viscosity of water as function of oil volume fraction. The measurements with fixed α are shown by the circles. The continuous measurements, for which α is changed during the experiments ($\omega_{\mathrm{IC}}/(2\pi)$ is fixed at 17.5 Hz), are shown as solid lines, while the dotted line is an experiment with $\omega_{\mathrm{IC}}/(2\pi) = 8$ Hz. The shaded area between the dashed vertical lines shows the ambivalence region, bounded by two catastrophic phase inversion, J1: *w-o* → *o-w* and J2: *o-w* → *w-o*. When water is the continuous phase, increasing α (á) leads to an increase in ν_{eff}, while when oil is the continuous phase decreasing α (b́), decreases ν_{eff}.

However, further increasing α in excess of 65% results in a dramatic drop in ν_{eff}, caused by the catastrophic phase inversion. Around the phase inversion $65\% < \alpha < 70\%$, ν_{eff} decreases by a factor of 6, resulting in a tremendous change of more than 40% in torque. Also, compared to the case of pure oil ($\alpha = 100\%$), we find that the case of $\alpha = 70\%$ has a lower effective viscosity, similar to other *w-o* emulsions [40]. We further note that our emulsions do not adhere to Einstein's [41] or Taylor's [42] viscosity correction factors around $\alpha = 0\%$ (where the viscosity increases faster than predicted) or $\alpha = 100\%$ (where the viscosity decreases rather than increases).

To further investigate what happens at the phase inversion we now quasistatically increase and decrease α, while keeping $\omega_{\mathrm{IC}}/(2\pi)$ fixed to 17.5 Hz, by slowly draining the setup at the bottom while filling it with oil or water from the top, see the red and blue curves in Fig. 3. The instantaneous value of α is obtained by recording the mass of the injected liquid and assuming that the liquid drained is a homogeneously mixed emulsion. At the end of the experiment, α was directly measured and found to be within 1% of the calculated value. We find that for both $d\alpha/dt > 0$ (red curves) and $d\alpha/dt < 0$ (blue curves) we see a catastrophic phase inversion for $\alpha = 72\%$ (J1) and $\alpha = 52\%$ (J2), respectively. The measurements for fixed α agree with those where we continuously change α, though the high ν_{eff} branch *(o-w)* was chosen by the system inside the ambivalence region. The emergence of the ambivalence region $52\% \leq \alpha \leq 72\%$ (shaded blue area in between vertical dashed lines in Fig. 3), is unexpected to exist for such high Ta [or equivalent Reynolds numbers of $\mathcal{O}(10^6)$]. One would expect that for such high Taylor numbers the system provides ample kinetic energy to freely explore the phase space, and thus arrive at the energetically most favorable state; however it has been shown before that turbulent TC flow is susceptible to hysteresis [34,43–45] and that emulsions also show hysteretic behavior [46]. For turbulent pipe flows [19,40,47] the width of the ambivalence region solely depends on the ratio of the dispersed phase injection rate and the total flow rate. We find that, for an injection rate of the dispersed phase of approximately 12.5 mL s^{-1} the ambivalence region gets slightly wider when Ta is decreased (illustrated from dashed to dotted boundaries in Fig. 3). This widening of the ambivalence region is thus delaying the phase inversion for both *o-w* and *w-o*, in contrast to the prediction of the extended Ginzburg-Landau model [16], from which one would expect independence of the Taylor number.

Which branch in the ambivalence region is chosen depends on the trajectory in parameter space used to reach $(\alpha, \omega_{\mathrm{IC}})$. Repeated experiments are found to give us repeatable results, such that a certain emulsion state (*w-o* or *o-w*) (and its corresponding low or high ν_{eff}) can be selected by performing the corresponding trajectory in phase space, opening possibilities for drag reduction for

the transport of emulsions that are within the ambivalence region. We label these phase inversions as catastrophic as these inversions completely change the morphology of the flow within a second, which results in a sharp increase (or decrease) of the torque by ≈35%. For both phase inversion 𝒥1 and 𝒥2 we see a sharp jump with the system, switching from a drag reduction to a severe drag increase, or vice versa.

The different responses seen in each of the branches in Fig. 3 demand a local view of the flow. Adding inclusions such as particles, bubbles, or immiscible fluids to a liquid can dramatically change its rheology [48,49]. Solids generally increase the effective viscosity [41,50], while small amounts of polymers [51], oil without surfactant [40], or gas [52–54] are known to reduce drag, yielding a lower effective viscosity than the original liquid phase. For the case of air lubrication, the current understanding suggests [53–56] that the Weber number, describing the deformability of the bubble, is of importance. The decrease in ν_{eff} for *w-o* emulsions (𝒷) could be a similar process as in bubble drag reduction [52–54], related to the deformability of the dispersed phase, for which large droplets are required. It was already found before that the droplet size in emulsions has a large impact on the rheology [57]. And, using the same reasoning, an increasing effective viscosity ν_{eff} (𝒶) could be connected with the presence of small and nondeformable droplets which could act as solidlike particles and therefore increase ν_{eff} [49,50,58].

Analyzing the size of our droplets is therefore paramount in order to see whether or not the above-mentioned effects could be of importance. Because of the metastable nature of the emulsion it quickly separates when driving is not continuously supplied, and therefore samples taken from the system and analyzed under a standard microscope do not have the same droplet sizes as those in the system while it is in operation. Consequently, we choose to bring the microscope to our apparatus and size the dispersed phase while in operation.

The optical arrangement is shown in Fig. 1(b). The dispersed droplets were visualized by the reflected light from their interface and no fluorescent dye was employed. We performed a sweep of α from 70% to 37% over the course of 16.5 min at a constant angular velocity of $\omega_{\mathrm{IC}}/(2\pi) = 8$ Hz while recording the torque and continuously imaging the droplets, see the dashed line in Fig. 3 for the ν_{eff} and Fig. 4 for the diameter of the droplets in the dispersed phase. A total of 14 500 frames were recorded and for each frame all the droplets were identified. We only observed simple emulsions and did not find any multiple emulsions (emulsions with deeper embeddings, e.g., w-o-w) [59]. The phase inversion can be seen in the dramatic jump in ν_{eff} in Fig. 3, but also directly in the mean diameter d of the dispersed phase in Fig. 4. We find that the phase inversion causes a 4× jump in ν_{eff} and the oil droplets were about 50% larger in radius (about 3.5× larger in volume) than the water droplets just before and after the phase inversion.

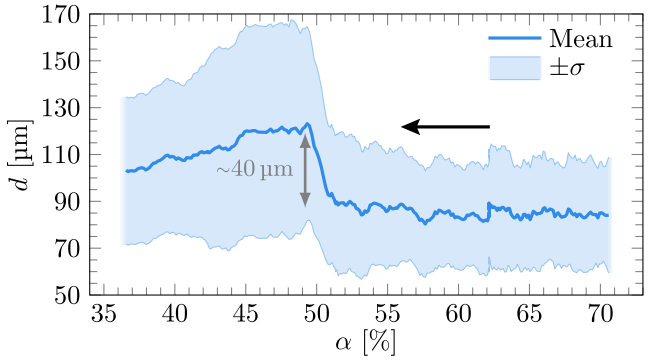

FIG. 4. Droplet diameter of the dispersed phase obtained using *in situ* microscopy for decreasing α for a rotational speed of $\omega_{\mathrm{IC}}/(2\pi) = 8$ Hz. A sharp jump in average diameter is found at the inversion point $\alpha \approx 50\%$, as is also visible in the measured torque (and from that ν_{eff}) as the dotted line in Fig. 3. The arrow indicates the direction of the α modification. Two example images are given in the Supplemental Material [60].

As in previous research [52–54], we calculate the Weber number to gauge the deformability and associated mobility of the droplets. In the turbulent case $\mathrm{We} = \rho u'^2 d/\gamma$, where ρ is the density of the mixture and u' is an estimate of the azimuthal velocity fluctuations based on previous research [61]. We find that We is 0.07 just before the jump, and 0.14 just after the jump, both well below unity. The requirement for bubbly drag reduction was found to be $\mathrm{We} > 1$ [52–54], so the traditional drag-reduction mechanism, invoking deformability of the bubbles, is likely not applicable for our high oil void fraction emulsions.

The size of the droplets is linked to the underlying flow structure, whose relevant length scale is the Kolmogorov length scale: $\eta_K = (\nu^3/\epsilon)^{1/4}$, comparing inertia and viscosity. Here ϵ is the turbulent energy dissipation rate. From this relation we find that $\eta_K = 12$ μm and 33 μm just before and after the jump. These values are both considerably smaller than the droplets we encountered. The relevant length scale in case of a dispersion in fact is the Hinze length scale [7], which compares inertia and capillarity: $d_{\mathrm{Hinze}} \approx 0.725(\gamma/\rho_{\mathrm{cont}})^{3/5}\epsilon^{-2/5} \approx 1320$ μm and 967 μm just before and after the jump, respectively. This is larger than what we optically found for the droplets. This estimate is based on dimensional analysis and different before and after the jump as ρ_{cont} of the carrier fluid abruptly changes from oil to water and ϵ also changes during the jump. Therefore, the first challenge is to understand the reason for the asymmetric jump in drag at the phase inversion. On the one hand, density differences might allow the heavier oil droplets to migrate closer to the IC than to the OC, while the lighter water droplets would do the opposite. On the other hand, oil adhesion to the metallic IC surface is known to increase when surrounded by water [62], while water droplets are not expected to adhere to the

acrylic OC surface surrounded by oil. These are two strong factors which could explain the asymmetry in the observed torque. Direct observation of these effects, to verify or falsify these hypotheses, are unfortunately impossible in the current experimental facility.

In summary, in this Letter we have studied the flow of metastable emulsions in an intensely sheared rotating flow. Exploiting the known scaling of the ultimate regime of Taylor-Couette flow, an effective viscosity of the emulsion can be measured, and thereby using the TC apparatus as a rheometer far beyond the conventional regime. With water as the continuous phase, the addition of oil droplets increases the drag of the system. Interestingly, drag is reduced when the water is injected in a continuous oil phase. At a critical volume fraction, a catastrophic phase inversion takes place, which dramatically changes the rheological properties. Using *in situ* microscopy we were able to obtain droplet sizes in the TC system while in operation. This showed that the jump observed in the torque can also be seen in the droplet size of the dispersed phase. The complex morphology on a microscopic scale with a wide size distribution of the dispersed phase was found to globally behave on the torque as if it were a Newtonian fluid. Our results demonstrate that we can select the emulsion type in the ambivalence region, which opens ways to achieve major drag reductions for the transport of emulsions. Our finding that an emulsion at high turbulent intensity behaves as if it were a Newtonian fluid is also highly relevant to the transport and mixing of emulsions, e.g., in oil recovery and the petrochemical industry.

We thank Raymond Bergmann, Nicolas Bremond, Sascha Hilgenfeldt, Dominik Krug, Henri Lhuissier, Andrea Prosperetti, Rian Ruhl, Vamsi Spandan, Peter Veenstra, Ruben Verschoof, Doris Vollmer, Jelle Will, and Jeff Wood for various stimulating discussions; Raymond Kip for help in the lab for preliminary work; and Gert-Wim Bruggert and Martin Bos for technical support. We also thank Guillaume Lajoinie and Tim Segers for assisting setting up the *in situ* microscopy measurements. This work was supported by Natural Science Foundation of China under Grants No. 11988102, No. 91852202, No. 11861131005, and No. 11672156, the Netherlands Organisation for Scientific Research (NWO) under VIDI Grant No. 13477, technology foundation STW, Foundation for fundamental research on matter, and multiscale catalytic energy conversion.

*d.lohse@utwente.nl
†chaosun@tsinghua.edu.cn
‡s.g.huisman@gmail.com

[1] S. Matar and L. F. Hatch, *Chemistry of Petrochemical Processes* (Elsevier, New York, 2001).
[2] D. K. Sarker, *Pharmaceutical Emulsions* (John Wiley & Sons, Ltd, New York, 2013).
[3] D. J. McClements, Food Emulsions: Principles, Practices, and Techniques (CRC Press, Boca Raton, 2004).
[4] J. Fink*Petroleum Engineer's Guide to Oil Field Chemicals and Fluids* (Elsevier, New York, 2015).
[5] J. Plasencia, B. Pettersen, and O. Jørgen Nydal, Pipe flow of water-in-crude oil emulsions: Effective viscosity, inversion point and droplet size distribution, J. Pet. Sci. Eng. **101**, 35 (2013).
[6] A. N. Kolmogorov, On the breakage of drops in a turbulent flow, Dokl. Akad. Nauk SSSR **66**, 825 (1949), https://ci.nii.ac.jp/naid/10021168703/en/.
[7] J. O. Hinze, Fundamentals of the hydrodynamic mechanism of splitting in dispersion processes, AIChE J. **1**, 289 (1955).
[8] R. Andersson and B. Andersson, On the breakup of fluid particles in turbulent flows, AIChE J. **52**, 2020 (2006).
[9] G. Zhou and S. M. Kresta, Correlation of mean drop size and minimum drop size with the turbulence energy dissipation and the flow in an agitated tank, Chem. Eng. Sci. **53**, 2063 (1998).
[10] R. Shinnar, On the behaviour of liquid dispersions in mixing vessels, J. Fluid Mech. **10**, 259 (1961).
[11] J. A. Boxall, C. A. Koh, E. D. Sloan, A. K. Sum, and D. T. Wu, Droplet size scaling of water-in-oil emulsions under turbulent flow, Langmuir **28**, 104 (2012).
[12] J.-L. Salager, L. Márquez, A. A. Peña, M. Rondón, F. Silva, and E. Tyrode, Current phenomenological know-how and modeling of emulsion inversion, Ind. Eng. Chem. Res. **39**, 2665 (2000).
[13] A. Perazzo, V. Preziosi, and S. Guido, Phase inversion emulsification: Current understanding and applications, Adv. Colloid Interface Sci. **222**, 581 (2015).
[14] P. Poesio and G. P. Beretta, Minimal dissipation rate approach to correlate phase inversion data, Int. J. Multiphase Flow **34**, 684 (2008).
[15] K. Ho Ngan, K. Ioannou, L. D. Rhyne, W. Wang, and P. Angeli, A methodology for predicting phase inversion during liquid–liquid dispersed pipeline flow, Chem. Eng. Res. Des. **87**, 318 (2009).
[16] K. Piela, G. Ooms, and J. V. Sengers, Phenomenological description of phase inversion, Phys. Rev. E **79**, 021403 (2009).
[17] N. Brauner and A. Ullmann, Modeling of phase inversion phenomenon in two-phase pipe flows, Int. J. Multiphase Flow **28**, 1177 (2002).
[18] L. Y. Yeo, O. K. Matar, E. S. Perez de Ortiz, and G. F. Hewitt, A description of phase inversion behaviour in agitated liquid–liquid dispersions under the influence of the Marangoni effect, Chem. Eng. Sci. **57**, 3505 (2002).
[19] K. Piela, R. Delfos, G. Ooms, J. Westerweel, R. V. A. Oliemans, and R. F. Mudde, Experimental investigation of phase inversion in an oil–water flow through a horizontal pipe loop, Int. J. Multiphase Flow **32**, 1087 (2006).
[20] H. Moradpour, A. Chapoy, and B. Tohidi, Phase inversion in water–oil emulsions with and without gas hydrates, Energy Fuels **25**, 5736 (2011).
[21] E. Dickinson, Interpretation of emulsion phase inversion as a cusp catastrophe, J. Colloid Interface Sci. **84**, 284 (1981).
[22] G. E. J. Vaessen, M. Visschers, and H. N. Stein, Predicting catastrophic phase inversion on the basis of droplet coalescence kinetics, Langmuir **12**, 875 (1996).

[23] E. Tyrode, J. Allouche, L. Choplin, and J.-L. Salager, Emulsion catastrophic inversion from abnormal to normal morphology. 4. following the emulsion viscosity during three inversion protocols and extending the critical dispersed-phase concept, Ind. Eng. Chem. Res. **44**, 67 (2005).

[24] D. P. M. van Gils, G.-W. Bruggert, D. P. Lathrop, C. Sun, and D. Lohse, The Twente turbulent Taylor-Couette (T^3C) facility: Strongly turbulent (multiphase) flow between independently rotating cylinders, Rev. Sci. Instrum. **82**, 025105 (2011).

[25] S. Grossmann, D. Lohse, and C. Sun, High–Reynolds Number Taylor-Couette Turbulence, Annu. Rev. Fluid Mech. **48**, 53 (2016).

[26] Lumenera, Lumenera LM165, 1392 px × 1040 px resolution, with 6.45 μm pixel size.

[27] Shin-Etsu Silicone Oil KF-96-1cSt.

[28] A. G. Kanellopoulos and M. J. Owen, Adsorption of sodium dodecyl sulphate at the silicone fluid/water interface, Trans. Faraday Soc. **67**, 3127 (1971).

[29] B. Eckhardt, S. Grossmann, and D. Lohse, Torque scaling in turbulent Taylor-Couette flow between independently rotating cylinders, J. Fluid Mech. **581**, 221 (2007).

[30] D. P. M. van Gils, S. G. Huisman, G.-W. Bruggert, C. Sun, and D. Lohse, Torque Scaling in Turbulent Taylor-Couette Flow with Co- and Counterrotating Cylinders, Phys. Rev. Lett. **106**, 024502 (2011).

[31] M. S. Paoletti and D. P. Lathrop, Angular Momentum Transport in Turbulent Flow between Independently Rotating Cylinders, Phys. Rev. Lett. **106**, 024501 (2011).

[32] S. G. Huisman, D. P. M. van Gils, S. Grossmann, C. Sun, and D. Lohse, Ultimate Turbulent Taylor-Couette Flow, Phys. Rev. Lett. **108**, 024501 (2012).

[33] R. Ostilla-Mónico, E. P. van der Poel, R. Verzicco, S. Grossmann, and D. Lohse, Boundary layer dynamics at the transition between the classical and the ultimate regime of Taylor-Couette flow, Phys. Fluids **26**, 015114 (2014).

[34] S. G. Huisman, R. C. A. van der Veen, C. Sun, and D. Lohse, Multiple states in highly turbulent Taylor–Couette flow, Nat. Commun. **5**, 3820 (2014).

[35] F. Wendt, Turbulente Strömungen zwischen zwei rotierenden konaxialen Zylindern, Arch. Appl. Mech. **4**, 577 (1933).

[36] D. P. Lathrop, J. Fineberg, and H. L. Swinney, Turbulent Flow Between Concentric Rotating Cylinders at Large Reynolds Number, Phys. Rev. Lett. **68**, 1515 (1992).

[37] G. S. Lewis and H. L. Swinney, Velocity structure functions, scaling, and transitions in high-Reynolds-number Couette-Taylor flow, Phys. Rev. E **59**, 5457 (1999).

[38] F. Ravelet, R. Delfos, and J. Westerweel, Experimental studies of turbulent Taylor-Couette flows: Single phase and liquid-liquid dispersions, arXiv:0707.1414.

[39] F. Ravelet, R. Delfos, and J. Westerweel, Experimental studies of liquid-liquid dispersion in a turbulent shear flow, Advances in Turbulence XI (Springer, Berlin Heidelberg, 2007), Vol. **331**.

[40] R. Pal, Pipeline flow of unstable and surfactant-stabilized emulsions, AIChE J. **39**, 1754 (1993).

[41] A Einstein, Eine neue Bestimmung der Moleküldimensionen, Ann. Phys. (N.Y.) **324**, 289 (1906).

[42] G. I. Taylor, The viscosity of a fluid containing small drops of another fluid, Proc. R. Soc. **138**, 41 (1932)

[43] C. D. Andereck, S. S. Liu, and H. L. Swinney, Flow regimes in a circular Couette system with independently rotating cylinders, J. Fluid Mech. **164**, 155 (1986).

[44] R. C. A. van der Veen, S. G. Huisman, O.-Y. Dung, H. L. Tang, C. Sun, and D. Lohse, Exploring the phase space of multiple states in highly turbulent Taylor-Couette flow, Phys. Rev. Fluids **1**, 024401 (2016).

[45] M. Gul, G. E. Elsinga, and J. Westerweel, Experimental investigation of torque hysteresis behaviour of Taylor–Couette flow, J. Fluid Mech. **836**, 635 (2018).

[46] J. Sjoblom, *Emulsions and Emulsion Stability: Surfactant Science Series/61* (CRC Press, Boca Raton, 2005), Vol. 135.

[47] K. Piela, R. Delfos, G. Ooms, J. Westerweel, and R. V. A. Oliemans, On the phase inversion process in an oil-water pipe flow, Int. J. Multiphase Flow **34**, 665 (2008).

[48] S. R. Derkach, Rheology of emulsions, Adv. Colloid Interface Sci. **151**, 1 (2009).

[49] J. J. Stickel and R. L. Powell, Fluid mechanics and rheology of dense suspensions, Annu. Rev. Fluid Mech. **37**, 129 (2005).

[50] D. Bakhuis, R. A Verschoof, V. Mathai, S. G Huisman, D. Lohse, and C. Sun, Finite-sized rigid spheres in turbulent Taylor-Couette flow: Effect on the overall drag, J. Fluid Mech. **850**, 246 (2018).

[51] C. M. White and M. G. Mungal, Mechanics and prediction of turbulent drag reduction with polymer additives, Annu. Rev. Fluid Mech. **40**, 235 (2008).

[52] T. H. van den Berg, D. P. M. van Gils, D. P. Lathrop, and D. Lohse, Bubbly Turbulent Drag Reduction is a Boundary Layer Effect, Phys. Rev. Lett. **98**, 084501 (2007).

[53] D. P. M. van Gils, D. N. Guzman, C. Sun, and D. Lohse, The importance of bubble deformability for strong drag reduction in bubbly turbulent Taylor-Couette flow, J. Fluid Mech. **722**, 317 (2013).

[54] R. A. Verschoof, R. C. A. van der Veen, C. Sun, and D. Lohse, Bubble Drag Reduction Requires Large Bubbles, Phys. Rev. Lett. **117**, 104502 (2016).

[55] J. Lu, A. Fernández, and G. Tryggvason, The effect of bubbles on the wall drag in a turbulent channel flow, Phys. Fluids **17**, 095102 (2005).

[56] V. Spandan, R. Verzicco, and D. Lohse, Physical mechanisms governing drag reduction in turbulent Taylor-Couette flow with finite-size deformable bubbles, J. Fluid Mech. **849**, R3 (2018).

[57] R. Pal, Effect of droplet size on the rheology of emulsions, AIChE J. **42**, 3181 (1996).

[58] F. De Vita, M. E. Rosti, S. Caserta, and L. Brandt, On the effect of coalescence on the rheology of emulsions, J. Fluid Mech. **880**, 969 (2019).

[59] F. Jahanzad, G. Crombie, R. Innes, and S. Sajjadi, Catastrophic phase inversion via formation of multiple emulsions: A prerequisite for formation of fine emulsions, Chem. Eng. Res. Des. **87**, 492 (2009).

[60] See Supplemental Material at http://link.aps.org/supplemental/10.1103/PhysRevLett.126.064501 for example images of the in situ microscopy experiment.

[61] R. Ezeta, S. G. Huisman, C. Sun, and D. Lohse, Turbulence strength in ultimate Taylor-Couette turbulence, J. Fluid Mech. **836**, 397 (2018).

[62] J. H. Clint and A. C. Wicks, Adhesion under water: Surface energy considerations, Int. J. Adhes. Adhes. **21**, 267 (2001).